

# **Controlling Graphene Ultrafast Hot Carrier Response from Metal-like to Semiconductor-like by Electrostatic Gating**

S.-F. Shi,<sup>1,2\*</sup> T.-T. Tang,<sup>1</sup> B. Zeng,<sup>1</sup> L. Ju,<sup>1</sup> Q. Zhou,<sup>1</sup> A. Zettl,<sup>1,2,3</sup> F. Wang<sup>1,2,3\*</sup>

<sup>1</sup> Department of Physics, University of California at Berkeley, Berkeley, 94720

<sup>2</sup> Material Science Division, Lawrence Berkeley National Laboratory, Berkeley, 94720

<sup>3</sup> Kavli Institute at University of California at Berkeley, Berkeley, 94720

## **Optical-pump THz-probe measurement setup**

We generate THz waves using air-plasma method<sup>1</sup> where 800 nm and 400 nm laser pulses (both with ~160 fs pulse duration and 1 kHz repetition rate) are simultaneously focused at the same spot in air. The generated THz radiation is collimated and focused onto our sample through a pair of parabolic mirrors. The transmitted THz wave is then re-collimated and focused onto a ZnTe crystal of 0.5 mm thickness, where the THz electrical field waveform is detected using electro-optic sampling.<sup>2</sup> The focused THz beam at our graphene sample has a diameter of 1 mm. For optical excitation, we use laser pulses with a pulse width of ~160 fs, a center wavelength at 800 nm, and a 3 mm diameter. Ultrafast time evolution of the transient THz signal is obtained by varying the time delay between optical pump and THz probe. We use ion-gel gating to control the carrier concentration in graphene and the resistance of the graphene is monitored in-situ during optical-pump THz-probe measurements. Ion-gel has been used previously<sup>3</sup> for efficient gating of graphene and is transparent in our THz spectral range (from 0.3 to 1 THz). In addition, our control measurements show that optical pumping of ion-gel on

fused silica reference substrate induces no measurable change of THz wave transmission. We purge the system with dry nitrogen during the measurement.

### **Sample preparation**

We grow single layer graphene on copper foil using CVD method and then transfer graphene to a fused silica substrate.<sup>4</sup> We use Raman spectroscopy to confirm that the graphene is single layer and to determine the Fermi energy of graphene at different gate voltages (through the G-peak Raman shift<sup>3,5</sup>). We evaporate 5/50 nm Ti/Au through a shadow mask to define source, drain and gate electrodes. The graphene piece between the source and drain electrodes is typically 5 mm by 5 mm.

### **Frequency dependence of the THz conductivity of graphene.**

Figure S1 displays frequency-dependent THz power transmitted through a bare fused silica substrate (red trace) and through an as-transferred graphene sample on fused silica (black trace). Their ratio (blue trace) is relatively flat, suggesting that graphene absorption, and therefore graphene conductivity, is relatively constant in the frequency range between 0.3-1.0 THz. This is consistent with a typical scattering rate of 4 THz in our CVD graphene.<sup>6</sup> Because of this largely constant THz conductivity over our frequency range, we can estimate the graphene conductivity directly through the magnitude of time-domain THz waveforms.

### **Electrical transport measurement.**

We monitor the resistance of the graphene device (shown in Fig. 2 of the main text) as we perform optical pump THz probe spectroscopy study, and the resistance as a function of gate voltage ( $V_g$ ) is shown in Figure S2. We determine that the charge neutral point (CNP) for this device is at  $V_g = 0.65$  V.

### **Determine graphene Fermi energy with Raman spectroscopy.**

We determine the Fermi energy of graphene using G peak position of Raman spectrum of graphene. Figure S3 plots the G-peak Raman shift a function of the relative gate voltage away from CNP (black dots). At high doping, the Fermi energy is directly proportional to the G-peak Raman shift with  $|E_F| = \frac{\Omega_G - 1578}{42\text{cm}^{-1}} (\text{meV})$ ,<sup>3,5</sup> and the values are shown in the right axis. G-peak shift can be nicely fitted by a square root dependence on gate voltage (red line), which gives  $|E_F| = (346\sqrt{V_g - V_{CNP}})[\text{meV}]$ . This equation allows us to estimate the Fermi energy at all gate voltages.

### **Drude weight at CNP and high doping**

At charge neutral point (CNP), higher electronic temperature leads to both more electrons in the conduction band and holes in the valence band, similar to that in a semiconductor. The net carrier concentration increase is  $\Delta n = \frac{\pi}{3} \left(\frac{kT_e}{\hbar V_F}\right)^2$ , and these extra charge carriers give rise to a large increase of Drude weight  $\Delta D = G_0 \times 2k(T_e - T_0)\ln 2$  (Eq. (3) in the main text). In highly doped graphene, however, higher electronic temperature mainly leads to a redistribution of charge carriers within the valence or

conduction band with no net change of charge carriers, similar to the behavior in a metal. The Drude weight change at high doping is therefore small, and it is mainly due to a shift of effective Fermi energy at elevated electronic temperatures (for fixed carrier concentration). This shift in Fermi energy as a function of temperature can be evaluated numerically for all doping levels (see the following discussion), and has a simple form of  $\Delta|E_F| \approx -\frac{\pi^2}{6} \left(\frac{kT_e}{E_F}\right)^2$  in highly doped graphene. This effect actually leads to a small decrease of Drude weight at increased electronic temperatures.

### **Fermi energy dependence on electron temperature at fixed carrier concentrations.**

As discussed in the main text, the effective Fermi energy of graphene is a function of electronic temperature at fixed carrier concentrations. The shift can be numerically calculated using conservation of number of carriers as:

$$\int_{-\infty}^{E_F(0K)} D(\epsilon) d\epsilon = \int_{-\infty}^{\infty} D(\epsilon) \frac{1}{1+\exp(\epsilon-E_F(T))} d\epsilon, \text{ where } D(\epsilon) = \frac{2}{\pi} \frac{|\epsilon|}{(\hbar v_F)^2} \text{ is the density of}$$

states for graphene. The numerically calculated effective Fermi energy at electronic temperature of 300 K and 600 K are shown in Figure S4. The shift of Fermi energy due to electronic temperature increase from 300 K to 600 K is also plotted. In the high doping limit, the shift of Fermi energy can be approximately obtained using Sommerfeld expansion as  $\Delta|E_F(T)| \equiv |E_F(T)| - |E_F(0K)| \approx -\frac{\pi^2}{6} \left(\frac{kT}{E_F(0K)}\right)^2$ . This behavior is

different from conventional two-dimensional electron gas, where the Fermi energy does not shift with elevated electronic temperature because it has a constant density of states.

### **Relation between $\Delta\sigma$ and $\Delta T_e$ .**

At the CNP  $\Delta\sigma$  is dominated by an increase of Drude weight, where  $\Delta D = G_0 \times 2k\Delta T_e \ln 2$ . At high doping, the conductivity change is dominated by a scattering rate increase. We can approximate the scattering rate increase  $\Delta\Gamma$ , and therefore conductivity change  $\Delta\sigma$ , to be linear with  $\Delta T_e$  in the perturbative region when  $kT_e \ll |E_F|$ .

Consequently, transient THz response in both cases scales linearly with  $\Delta T_e$ . The power law scaling of  $\Delta E/E$  in the main text can be understood as the power law scaling of electronic temperature increase  $\Delta T_e$ .

### **Hot carrier temperature at different pump fluence and Fermi energies.**

The electronic temperature of hot carriers can be calculated if we know the fraction of absorbed energy is retained in the hot carriers. Using the fitting result in Fig. 3(b) of the main text and the heat capacitance of the Dirac electrons, we obtain the hot electron temperature in graphene for both the CNP and high doping cases as a function of pump fluence as shown in Fig. S5. It is clear that the optical pump heats up electrons more efficiently in charge neutral graphene.

We also show the optical pump induced THz field transmission change at high fluence limit in log-log scale (same data as in Figure 3b) to better show the power law dependence on fluence. It is noted that the change at -500 meV (black squares) has slightly different slope compared with the change at -370 meV (red dots). This is likely due to the fact that the optical excitation induced THz transmission change is not fully saturated at the fluence of  $45 \mu\text{J}/\text{cm}^2$  yet at the Fermi energy of  $-500 \text{ meV}$ .

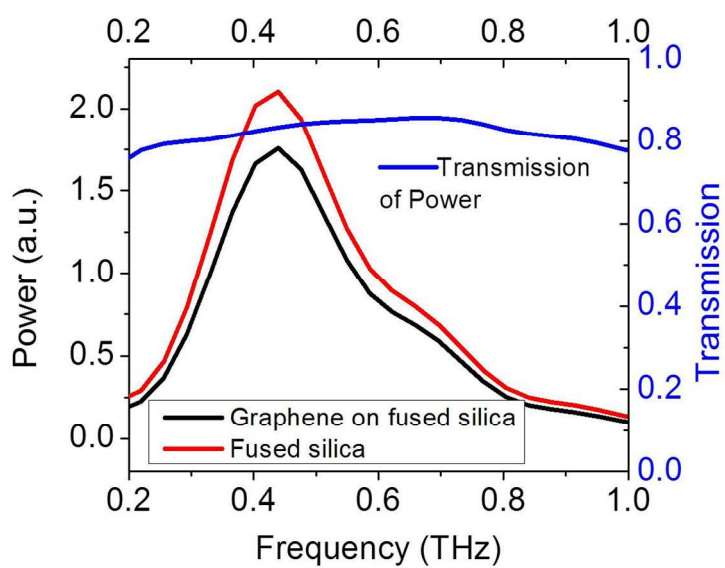


Figure S1. Fourier transform of THz wave transmitted through a fused silica reference substrate (red) as well as as-transferred CVD graphene on fused silica. The THz power transmission through graphene (blue) is relatively flat over the frequency we study.

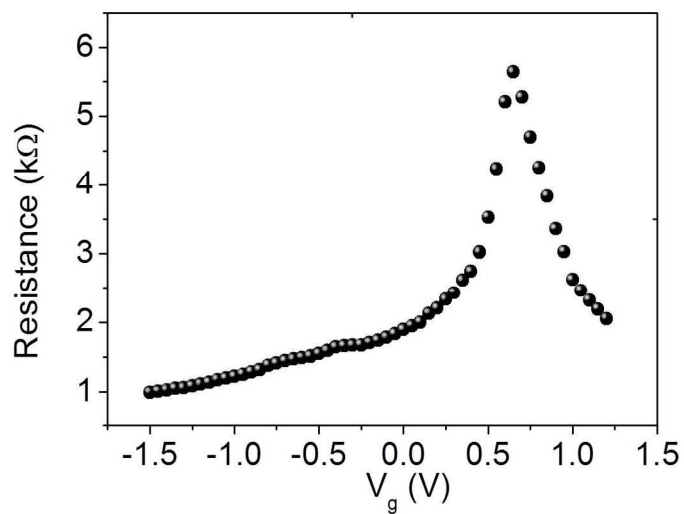


Figure S2. Resistance of the graphene device shown in the Fig. 2 (the main text) as a function of the gate voltage. The resistance is at maximum when the gate voltage is at 0.65 V.

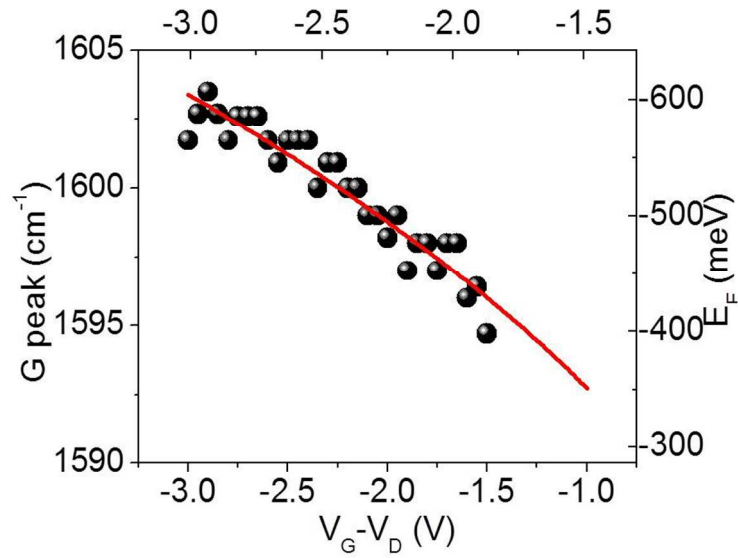


Figure S3. G peak position of the Raman spectrum of the gated graphene device as shown in Fig. 2 (the main text) in the high doping regime. Experimental data (black dots) are fitted (red curve) assuming a square root dependence of gate voltage away from charge neutral point (CNP). Fermi energy of graphene can be extracted from a linear dependence on the G peak position<sup>3,5</sup>

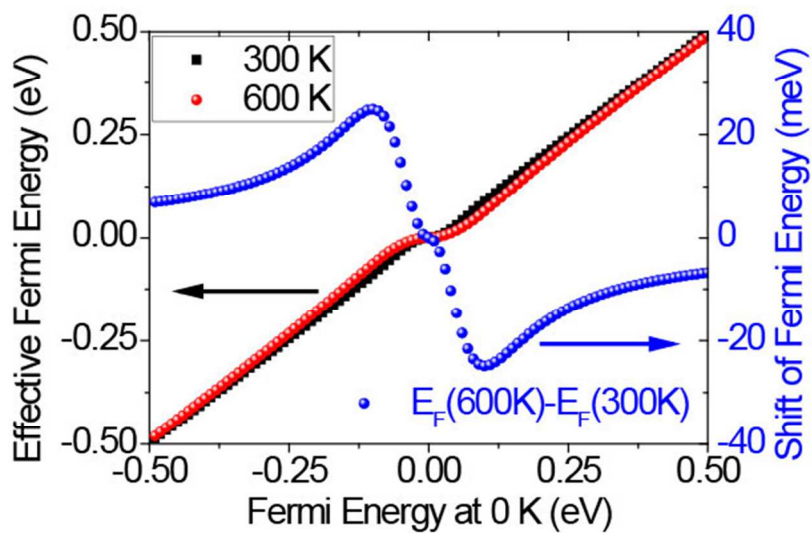


Figure S4. Numerically calculated effective Fermi energy at 300 K (black) and at 600 K (red) as a function of Fermi energy at zero temperature. Fermi energy shift due to elevated electronic temperature (blue) can be obtained as the difference between these two.

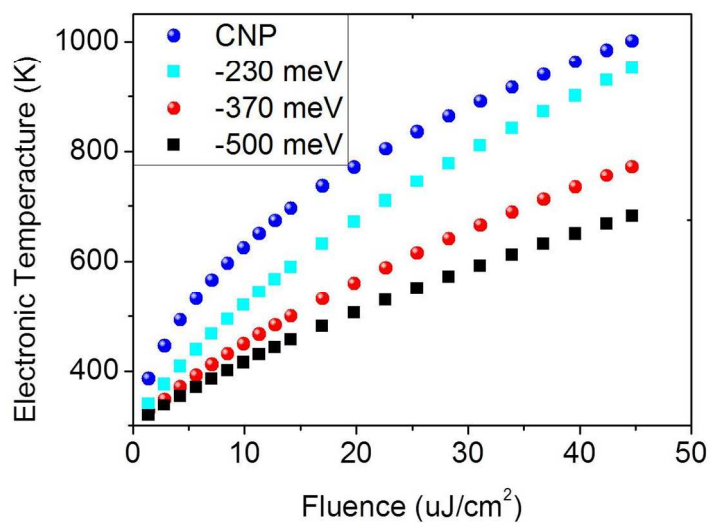


Figure S5. Numerically calculated electronic temperature as a function of excitation fluence for graphene with different Fermi energies. We use the fitting result from Fig. 3(b) for this calculation.

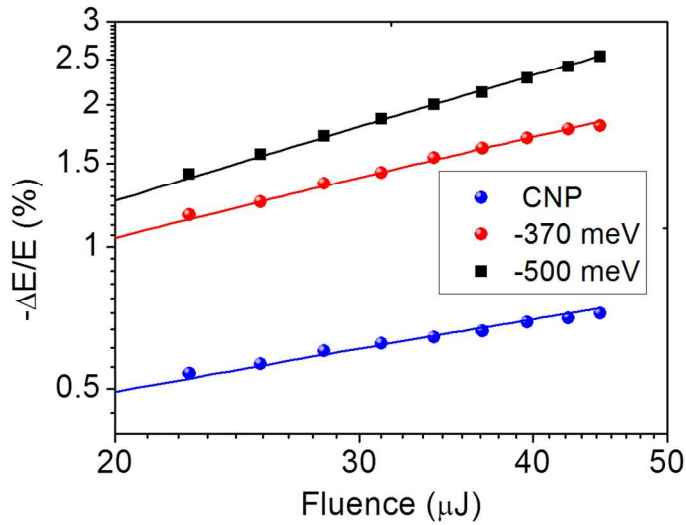


Figure S6. Absolute photon-induced change of THz field transmission as a function of excitation fluence. This is a log-log scale plot of Fig. 3b in the main text to better show the power law dependence in the high fluence limit.

## Reference

- <sup>1</sup> Xie, X.; Dai, J.; Zhang, X. C. *Phys. Rev. Lett.* **7**, 075005 (2006).
- <sup>2</sup> Nahata, A.; Huston, D. H.; Heinz, T. F.; Wu, C. *Appl. Phys. Lett.* **68**, 150 (1996).
- <sup>3</sup> Chen, C-F.; Park, C.-H.; Boudouris, B. W.; Horng, J.; Geng, B.; Girit, C.; Zettl, A.; Crommie, M. F.; Segalman, R. A.; Louie, S. G.; Wang, F. *Nature* **471**, 617 (2012).
- <sup>4</sup> Li, X.; Cai, W.; An, J.; Kim, S.; Nah, J.; Yang, D.; Piner, R.; Velamakanni, A.; Jung, I.; Tutuc, E.; Banerjee, S. K.; Colombo, L.; Ruoff, R. S. *Science* **324**, 1312 (2009).
- <sup>5</sup> Yan, J.; Zhang, Y.; Kim, P.; Pinczuk, A. *Phys. Rev. Lett.* **98**, 166802 (2007).

---

<sup>6</sup> Horng, J.; Chen, C.-F.; Geng, B.; Girit, C.; Zhang, Y.; Hao, Z.; Bechtel, H.A.;  
Martin, M.; Zettl, A.; Crommie, M.F.; Shen, Y. R.; Wang, F. *Phys. Rev. B.* **83**, 165113  
(2011).